Accepted Manuscript

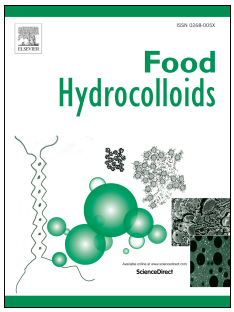

A further understanding of the multi-scale supramolecular structure and digestion rate of waxy starch

Dongling Qiao, Fengwei Xie, Binjia Zhang, Wei Zou, Siming Zhao, Meng Niu, Rui Lv, Qian Cheng, Fatang Jiang, Jie Zhu

PII: S0268-005X(16)30485-4

DOI: 10.1016/j.foodhyd.2016.10.041

Reference: FOOHYD 3659

To appear in: *Food Hydrocolloids*

Received Date: 26 September 2016

Revised Date: 20 October 2016

Accepted Date: 25 October 2016

Please cite this article as: Qiao, D., Xie, F., Zhang, B., Zou, W., Zhao, S., Niu, M., Lv, R., Cheng, Q., Jiang, F., Zhu, J., A further understanding of the multi-scale supramolecular structure and digestion rate of waxy starch, *Food Hydrocolloids* (2016), doi: 10.1016/j.foodhyd.2016.10.041.

A further understanding of the multi-scale supramolecular structure and digestion rate of waxy starch

Dongling Qiao [a, b,f], Fengwei Xie [c], Binjia Zhang [a,*], Wei Zou [d], Siming Zhao [a], Meng Niu [a], Rui Lv [a], Qian Cheng[a], Fatang Jiang [b], Jie Zhu [e,f]

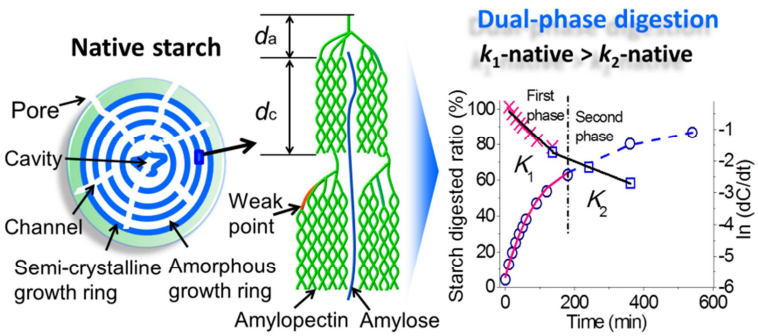

The multi-scale supramolecular structure of starch closely relates to its digestion rate.

* Corresponding author. Tel.: +86 27 87288375; fax: +86 27 87288375. *E-mail address*: zhangbj@mail.hzau.edu.cn (B. Zhang).

A further understanding of the multi-scale supramolecular structure and digestion rate of waxy starch

Dongling Qiao [a, b,f], Fengwei Xie [c], Binjia Zhang [a,*], Wei Zou [d], Siming Zhao [a], Meng Niu [a], Rui Lv [a], Qian Cheng[a], Fatang Jiang [b], Jie Zhu [e,f]

[a] *College of Food Science and Technology, Key Laboratory of Environment Correlative Dietology (Ministry of Education), Huazhong Agricultural University, Wuhan 430070, China.*

[b] *Glyn O. Philips Hydrocolloid Research Centre at HUT, Hubei University of Technology, Wuhan 430068, China*

[c] *School of Chemical Engineering, The University of Queensland, Brisbane, Qld 4072, Australia*

[d] *Centre for Nutrition and Food Sciences, Queensland Alliance for Agriculture and Food Innovation, The University of Queensland, Brisbane, Qld 4072, Australia*

[e] *College of Chemistry and Environmental Engineering, Dongguan University of Technology, Dongguan 523808, China*

[f] *Guangdong Province Key Laboratory for Green Processing of Natural Products and Product Safety, South China University of Technology, Guangzhou 510640, China*

[*] Corresponding author. Tel.: +86 27 87288375; fax: +86 27 87288375. *E-mail address*: zhangbj@mail.hzau.edu.cn (B. Zhang).

Abstract: This work concerns how the multi-scale supramolecular structure of starch relates to its digestion rate from a view of structural heterogeneity. The untreated granule starch displayed a dual-phase digestion pattern, ascribed to two digestible fractions within the heterogeneous multi-scale structure of starch, which had prominently different digestion rates. Not only amorphous starch but also part of molecular orders (crystallites with flaws) were digested at a same rate k_1 at the first phase; densely-assembled starch including orders with fewer flaws was digested at a rather slow rate k_2 (*ca*. 2/5 of k_1) at the second phase. When alkali altered the heterogeneous supramolecular structure of starch, the digestion behaviors were also changed. The 0.1% (w/v) alkali solution slightly disrupted the starch multi-scale structure, which reduced the molecular orders, disrupted the lamellae, weakened the molecular organization within growth rings, and enlarged the granule pores. Then, part of resistant starch was transformed into slowly-digestible fraction with a digestion rate close to k_2. In contrast, when stronger (0.5% w/v) alkali was used, the starch multi-scale structure was more apparently disrupted, causing even granule swelling. This structural change resulted in a triple-phase digestion with three different digestion rates. Moreover, especially with stronger alkali, along with the structural disruption, some orders with a higher thermal stabilty emerged and reduced the accessibility of starch molecules to the enzyme. In this case, the digestion rate decreased with the treatment time.

Keywords: Starch; Multi-scale; Supramolecular structure; Digestion rate

1. Introduction

The digestion of food biopolymers, *e.g.*, starch, and protein, always involves enzymes that depolymerize the macromolecular substances into oligomer/monomer units under certain kinetics. Starch, as a storage biopolymer in higher plants, is a key carbohydrate providing energy for humans (Juansang, Puttanlek, Rungsardthong, Puncha-arnon, & Uttapap, 2012). Starch contains two major D-glucans, *i.e.*, amylose and amylopectin (Liu, Halley, & Gilbert, 2010). These two polymers assemble on different scales in the starch granule to form a multi-scale supramolecular structure with heterogeneity, mainly including the whole granule (< 1 μm-100 μm), the growth rings (100-400 nm), and the semicrystalline lamellae (9-10 nm) (Perez & Bertoft, 2010; Zhang, et al., 2015b; Zhang, et al., 2014b). The digestion of starch releases glucose, which relates to metabolic diseases, *e.g.*, Type II diabetes, obesity and cardiovascular diseases (Robertson, Currie, Morgan, Jewell, & Frayn, 2003; Zou, Sissons, Gidley, Gilbert, & Warren, 2015). Thus, to maintain people's health, considerable attention has been paid to the modulation of starch digestibility (*e.g.*, digestion rate and degree) (Chen, et al., 2016).

Despite for human diets starch is usually consumed after processing, granule starch is also used widely, for example for low-moisture foods (*e.g.*, biscuits) (Blazek & Gilbert, 2010), fruits, vegetables, animal feeds, and industrial conversions. For the granule starch digestion, the enzyme firstly diffuses toward and binds the substrate, followed by the adsorption and catalytic events (Bertoft & Manelius, 1992). The tight assembly of starch molecular chains in the multi-scale supramolecular structure of granule starch can suppress the enzyme diffusion/absorption and hydrolysis (Bertoft, et al., 1992). The digestion rate of untreated granule starch by amylase is normally several times lower than that of starch after processing such as cooking (Blazek, et al., 2010; Noda, et al., 2008; Zhang, Dhital, & Gidley, 2013). This lower digestion rate was proposed due to the existence of ordered structure in

granule starch before processing, which reduces the accessibility of starch molecules to the digestive enzymes. However, an increasing number of studies have shown contradictory results, revealing that the degree of molecular disassembly (structural disorganization) of granule starch during processing, such as gelatinization, only has little effects on starch digestibility including digestion rate (Chung, Lim, & Lim, 2006; Tamura, Singh, Kaur, & Ogawa, 2016; Wang, Sun, Wang, Wang, & Copeland, 2016). Hence, it is still inconclusive how the multi-scale structure of granule starch governs the digestion rate of starch.

As mentioned above, the multi-scale supramolecular structure of granule starch is heterogeneous. That is, starch molecules packed in the structures on multiple scales have varied degrees of compactness and thus show structural heterogeneity. This heterogeneity probably endows starch molecules assembled in granule starch with prominently different susceptibilities to enzyme hydrolysis (*i.e.*, digestion rates). However, though numerous reports evaluate the effect of starch structure, such as crystallites and helices, on starch digestibility (Zhang, et al., 2014a; Zhang, Chen, Zhao, & Li, 2013), there is limited understanding of how the multi-scale supramolecular structure of granule starch relates to its digestion rate from a structural heterogeneity view. Therefore, based on this view, we may better explore the links between specific structures of granule starch and starch digestion rate, which is crucial for the rational development of starchy foods with tailored digestibility.

This work was aimed at disclosing the relationship between the multi-scale supramolecular structure of granule starch and its digestion rate from a view of structural heterogeneity. Regarding this, the multi-scale structural features of the starch were interrogated by different techniques. The digestibility (digestion rate) of the starch was evaluated using a modified *in vitro* method (Zou, et al., 2015). Besides, alkali was used to vary the multi-scale supramolecular structure of starch with heterogeneity. Intense alkali can quickly disrupt the starch structure and prominently degrades starch molecules (Han & Lim,

2004) due to the β-elimination of reducing semi-acetal groups. In this work, we chose to use moderate alkali treatment (alkali concentrations: 0.1% w/v and 0.5% w/v) with long-term periods (6 and 12 days) to modify the starch structure without degradation of starch molecules (Cai, et al., 2014; Jiang, et al., 2014; Nadiha, Fazilah, Bhat, & Karim, 2010; Praznik, Buksa, Ziobro, Gambuś, & Nowotna, 2012; Wang & Copeland, 2012). Also, waxy starch has advantages for this study, as its granule has a loose surface (typically with pores) and an interior structure with weak-points. This makes any evolutions in the supramolecular structure and thus in the digestion rate of starch induced by alkali more apparent.

2. Materials & methods

2.1 Materials

Waxy maize starch was purchased from Penford Australia Pty Ltd. (Lane Cove, NSW, Australia). The starch has an amylose content of *ca*. 3%, as measured using the iodine colorimetric method (Tan, Flanagan, Halley, Whittaker, & Gidley, 2007). A moisture analyzer (MA35, Sartorius Stedim Biotech GmbH, Germany) was used to measure the moisture content of each starch sample. Sodium hydroxide, sodium azide, and ethanol were of analytical grade, and were purchased from Tianjin Kemeou Chemical Reagent Co., Ltd. (China). α-Amylase from porcine pancreas (A-3176; 23 unit amylase/mg solid; one unit liberates 1.0 mg of maltose from starch in 3 min at 37 °C), phosphate buffered saline tablet (P4417-100TAB), 4-hydroxybenzhydrazide (PAHBAH, H9882) and maltose (M-9171) were supplied by Sigma-Aldrich Pty Ltd. (Castle Hill, NSW, Australia).

2.2 Preparation of alkali-treated starch

Approx. 10.0 g of the starch was added into 150 mL sodium hydroxide aqueous solution at a concentration of 0.1% (w/v) or 0.5% (w/v), together with 0.1% (w/v) sodium azide as a chemical preservative. The starch slurries were kept at 35 °C for 6 or 12 days with

intermittent shaking to fully re-suspend the starch. After the treatment, the starch was washed with deionized water, followed by 95% ethanol (Jiang, et al., 2014; Wang, et al., 2012), and centrifuged for 3-5 times until the slurry became neutral. The starch sediment was dried in an oven at 35 °C for 48 h. In the following, codes typical as "S-0.5-12" was used, where "S" indicates the starch, "0.5" denotes the concentration (%) of sodium hydroxide, and "12" means the days of treatment. Also, "S" represents the native (*i.e.*, untreated) starch.

2.3 Scanning electron microscopy (SEM)

The granule morphology of the starch was observed using a Zeiss Merlin Ultra Resolution SEM (Carl Zeiss AG, Oberkochen, Germany). The samples were mounted on a metal stage and then coated with iridium. The images were obtained at an accelerating voltage of 2 kV.

2.4 Laser diffraction analysis

Granule size distribution was evaluated by a Malvern Mastersizer 2000 laser diffraction analyzer (Version 5.22, Malvern, UK). The obscuration value was 12% to 17%, with a pump speed 2050 r/min. The refractive index of the starch and the dispersing reagent ethanol was 1.54 and 1.36, respectively.

2.5 Synchrotron small-angle X-ray scattering (SAXS)

SAXS measurements were performed on the SAXS/WAXS beamline (flux, 1013 photons/s) at the Australian Synchrotron (Clayton, Vic, Australia), at a wavelength λ = 1.47 Å. The starch suspensions with a starch concentration of 40wt% were placed on a multi-well stage, and then the SAXS data were recorded for an acquisition time of 1 s. The scattering of pure water with Kapton tape (5413 AMBER 3/4IN X 36YD, 3M, USA) on the stage window was used as the background data. All the data were background subtracted and

normalized. The data in the range of $0.0020 < q < 0.20$ Å^{-1} were used as the SAXS pattern, where $q = 4\pi\sin\theta/\lambda$, in which 2θ is the scattering angle and λ the X-ray wavelength.

For the SAXS patterns, the data in the range of $0.0020 < q < 0.04$ Å^{-1} were fitted using a unified model Eq. (1) (Zhang, et al., 2015b).

$$I(q) = G\exp\left(-\frac{R_g^2 q^2}{3}\right) + C\left(\frac{\left(\mathrm{efr}\left(\frac{qR_g}{\sqrt{6}}\right)\right)^3}{q}\right)^{\delta} \quad (1)$$

Here, G is the pre-factor of the Guinier function corresponding to a radius R_g; and C and δ are the pre-factor and the exponent of the power-law function, respectively.

SAXS data in the lamellar peak range ($0.04 < q < 0.20$ Å−1) were fitted using a power-law plus Gaussian function (Zhang, et al., 2015b), as shown in Eq. (2) below.

$$I(q) = B + Pq^{-\alpha} + \frac{A\sqrt{\ln 4}}{W\sqrt{\frac{\pi}{2}}}\exp\left(-\frac{2\ln 4(q - q_0)^2}{W^2}\right) \quad (2)$$

Where the first term B is the background; the second term is the power-law function where P is the power-law pre-factor and α is the power-law exponent; the third term is a Gaussian function where A is the peak area, W (Å^{-1}) the full width at half maximum (FWHM) of peak in reciprocal space, and q_0 (Å^{-1}) the peak center position (Blazek, et al., 2010; Witt, Doutch, Gilbert, & Gilbert, 2012). Data fitting was performed using least-square refinement in the NCNR analysis macros.

The one-dimensional (1D) correlation function $L(r)$ (Kuang, et al., 2017; Yang, et al., 2016; Zhang, Chen, Li, Li, & Zhang, 2015a), as given in Eq. (3) and **Fig. S1** (supplementary material), was used to study the parameters of the starch lamellar structure.

$$L(r) = \frac{\int_0^\infty I(q)q^2 \cos(qr)\, dq}{\int_0^\infty I(q)q^2 dq} \quad (3)$$

In which, r (nm) is the distance in real space. d is the second maximum of $L(r)$ (*i.e.*, the thickness of semi-crystalline lamellae). d_a, the average thickness of amorphous lamellae within semicrystalline lamellae, is acquired by the solution of the linear region and the flat $L(r)$ minimum (see **Fig. S1** in supplementary material) (Zhang, et al., 2015b). d_c, the average thickness of crystalline lamellae within semi-crystalline lamellae, is calculated by $d_c = d - d_a$.

2.6 Polarized light microscopy

A polarization microscope equipped with a CMOS camera was used, and the magnification was × 400 (40 × 10). For the observation, suspensions with 0.5% starch were prepared in glass vials.

2.7 X-ray diffraction (XRD)

The crystalline structure of the starch was evaluated using an X-ray powder diffractometer (D8 Advance, Bruker AXS Inc., Madison, WI, USA), operated at 40 kV and 30 mA. XRD patterns were acquired for a 2θ range of 4-40°, with a step size of 0.02° and a step rate of 0.5 s per step. The relative crystallinity (X_c, %) was calculated using PeakFit software (Ver. 4.12), according to Eq. (4).

$$X_c = \frac{\sum_{i=1}^{n} A_{ci}}{A_t} \quad (4)$$

Where A_{ci} is the area under each crystalline peak with index i; and A_t is the total area of the diffraction pattern.

2.8 Differential scanning calorimetry (DSC)

The thermal behaviors of the starch were measured using a PerkinElmer DSC 8500. A high-pressure stainless steel pan with a gold-plated copper seal was used. The samples (*ca.* 12-15 mg) with 70% moisture content were heated from 30 to 120 °C at a rate of 10 °C /min. All results were reported as averages of three replicates.

2.9 *In vitro* digestion

Due to the complexity of human digestive process with multiple enzymes and the hormonal control of these enzymes, the investigation of *in vivo* starch digestion is challenging and thus is typically mimicked by *in vitro* methods conducted by one or more enzymes (Hasjim, Lavau, Gidley, & Gilbert, 2010). *In vitro* digestion of starch was carried out in triplicate. A centrifuge tube with 90.0 mg of starch and 16.0 mL of deionized water was incubated at 37 °C. Then, 5.0 mL of phosphate buffer solution (PBS; one phosphate buffered saline tablet dissolved in 200 mL of deionized water yields 0.01 M phosphate buffer, 0.0027 M potassium chloride and 0.137 M sodium chloride, pH 7.4, at 25 °C) with 9.0 mg of porcine α-amylase (23 unite amylase/mg solid) was pipetted into the tube. Afterward, 100.0 μL of the digestion solution was collected at each time point and transferred into a prepared centrifuge tube containing 900.0 μL of 0.3 mol/L Na_2CO_3 solution to terminate enzymatic digestion. 1.0 mL of the mixed solution was then centrifuged at 8000 *g* for 10 min before 100.0 μL of supernatant was pipetted into 1.0 mL of PAHBAH solution (prepared by dissolving 500.0 mg of PAHBAH powder into 10.0 mL of 0.5 M HCl, followed by addition of 90.0 mL of 0.5 M NaOH). The resultant solution was incubated in boiling water for 5 min. After cooling to ambient temperature, the absorbance at 410 nm (McDougall, et al., 2005; Nwosu, et al., 2011) was recorded by using a UV-1700 spectrophotometer (Shimadzu Corp., Kyoto, Japan). Maltose solution (1.0 mol/L) was used as a standard for quantifying the amount of reducing sugar released during starch digestion. The percentage of digested starch (maltose equivalent released) was calculated according to Eq. (5).

$$SD(\%) = A_{sample} \times \frac{100\mu L \times 1.0mg/L}{A_{maltose}} \times 10 \times 210 \times \frac{100\%}{90mg} \times \frac{324}{342} \quad (5)$$

202

203 Here, *SD* is the percentage of starch digested; and A_{sample} and $A_{maltose}$ are the absorbance values for
204 the starch digestion solution and maltose standard, respectively. The value of 10 × 210 is the
205 computational multiple from 100.0 μL aliquots to 21.0 mL reaction solution, and 324/342 is the
206 transformation coefficient from maltose to starch in weight.

207 *2.10 First-order kinetics*

208 Other than the commonly-used first-order kinetic model (Eq. (6)), the accompanying logarithm of
209 the slop (LOS) plot (Poulsen, Ruiter, Visser, & Iversen, 2003; Zou, et al., 2015) (Eq. (7)) was used to
210 fit the digestion data for describing the sequential first-order kinetics of the starch digestion.

211

$$C_t = C_\infty(1 - e^{-k \cdot t}) \quad (6)$$

$$\ln\frac{dC_t}{dt} = -k \cdot t + \ln(C_\infty \cdot k) \quad (7)$$

212

213 Where C_t (%) is the proportion of the starch digested at a given time (t (min)), C_∞ (%) is the
214 estimated percentage of the starch digested at the end point of a digestion stage, and k (min^{-1}) is the
215 coefficient of starch digestion rate. The calculated digestion data ($ln[(C_{i+2} - C_i)/(t_{i+2} - t_i)]$) at each
216 time point ($(t_{i+2} + t_i)/2$), except the last two points, was used to obtain the LOS pattern and the
217 related fit curve.

218 The LOS plot visibly reveals the number of starch digestion phases throughout the whole reaction
219 period according to the changes in the slope of digestion pattern ($ln(dC_t/dt)$) *vs.* time (t). Hence,
220 using the LOS plot derived from digestion data, the different digestion stages with different digestion
221 rate coefficients (k) could be shown. The obtained k and C_∞ were used to plot the starch digestion

curve according to Eq. (6) to compare the original data with the fitted starch digestion curves generated by the fit model.

2.11 Statistical Analysis

Data were reported as means ± standard deviations and were analyzed by one-way ANOVA and multiple comparison tests with the least significant difference using the IBM SPSS software ver. 20.0 (Chicago, IL, USA). A statistical difference of $P < 0.05$ was considered to be significant. Linear regression fitting was carried out using Microsoft Excel 2010 (Redmond, WA, USA).

3. Results and Discussion

3.1 Granule morphology and size

The SEM micrographs of the starch granules before and after alkali treatment are presented in **Fig. 1**. Untreated starch granules showed a relatively smooth and compact surface with typical pores. The 0.1% concentration alkali increased the surface roughness and enlarged the surface pores for the starch granules. When 0.5% alkali was used, part of starch granules were broken. Regardless of the alkali concentration, the increased treatment time induced negligible changes to the granule morphology.

Table 1 shows the granule size distribution of the starch and its alkali-treated samples. After the 0.1% alkali treatment, a decrease was seen in the granule fraction in the size (diameter) range of > 28 µm (P_{D3}), accompanied by increases in the granule fractions in the size ranges of < 7 µm (P_{D1}) and 7-28 µm (P_{D2}). The longer treatment time (12 days) induced a further increase in the proportion of small size (< 7 µm) granules. This indicates that the mild (0.1%) alkali solution reduced the starch granule size rather than induced granule swelling.

With a stronger (0.5%) alkali treatment, there was an apparent increase in the starch granule size fraction of > 28 µm but a decrease in that of 7-28 µm; the proportion of starch granule size fraction of < 7 µm kept constant. These data suggested that the 0.5% alkali treatment induced granule

swelling and increased the granule size of the starch. However, as the treatment time increased, the increase in the granule size fraction of > 28 μm and the decrease in that of 7-28 μm became less prominent. Regarding this, we suggest that concurrent granule swelling and molecule leaching occurred during the 0.5% alkali treatment. This stronger alkali treatment for 6 days mainly swelled the starch granules (*i.e.*, increased granule size); a longer treatment time (12 days) could reduce the increase of granule size by inducing molecular leaching from the superficial and interior regions of the starch granule.

3.2 Large-scale structure

Fig. 2A-E presents the SAXS patterns of native and alkali-treated starches. **Table 1** records the parameters of the large-scale structures for the starch including growth rings and blocklets. The starch samples showed typical surface fractal scattering (*i.e.*, power exponent $\delta_1 > 3$) at very low q values of *ca*. 0.0020-0.01 $Å^{-1}$. This was ascribed to interfacial scattering from growth rings with a radius of gyration (R_{g1}) *ca.* 1000 Å (Zhang, et al., 2015b). After the alkali treatment especially at high concentration (0.5%), there was a reduction in δ_1 (with slightly changed R_{g1}), indicating a decrease in the compactness of molecular organization of the growth rings.

By fitting the SAXS data in second-level q-range (**Fig. 2A-E** and **Table 1**), a structure with a R_{g2} of approx. 195 Å was revealed, corresponding to the blocklets and mass fractal structure ($\delta_2 < 3$) within the growth rings (Doutch & Gilbert, 2013). A reduction in R_{g2} was seen after 0.1% alkali treatment, indicating that this mild alkali centripetally removed starch molecules from blocklets and mass fractals. With the 0.5% alkali treatment, a prominent increase in R_{g2} was seen, mainly related to the alkali-induced molecule swelling in the blocklets and mass fractals. Besides, similar to the granule size evolution, the increase in treatment time with 0.5% alkali slightly weakened the degree of increase in R_{g2}, due to the alkali-induced molecule leaching from the blocklets and mass fractals.

3.3 Lamellar structure

From **Fig. 2**, a scattering peak at *ca.* 0.06 $Å^{-1}$ was seen for the semicrystalline lamellae (Zhang, et al., 2015b) of the starch samples. **Table 2** lists the fitted lamellar parameters. Both the peak area A_{peak} and the peak intensity I_{peak} showed a moderate increase after the 0.1% alkali treatment but an evident reduction with the 0.5% alkali treatment. This evolution in I_{peak} was also confirmed by the brightness changes in the 2D scattering circle of the semicrystalline lamellae in the inserted graphs in **Fig. 2A-E**.

While the peak area indicates the degree of lamellae ordering (Zhang, et al., 2014d), the peak intensity positively correlated to the electron density difference $\Delta\rho$ ($=\rho_c - \rho_a$) between the crystalline lamellae (ρ_c) and the amorphous lamellae (ρ_a). Hence, it is concluded that although the 0.1% alkali mildly affected the whole semicrystalline lamellae, it preferably altered the amorphous lamellae rather than the crystalline lamellae, leading to increases in the lamellae ordering and $\Delta\rho$; the 0.5% alkali effectively disrupted especially the crystalline lamellae to reduce the lamellae ordering and $\Delta\rho$. With the increased treatment time, although the 0.1% alkali further increased A_{peak} and I_{peak}, the 0.5% alkali less effectively reduced these two parameters. This indicates that the 0.5% alkali induced molecular out-phasing and/or swelling in particular for the amorphous lamellae, and/or the realignment of starch molecular chains into the crystalline lamellae. Either scenario could offset part of decreases in lamellae ordering and $\Delta\rho$ with the 0.5% alkali treatment for a longer time (12 days).

According to the paracrystalline model (Cameron & Donald, 1993), while the major effect of increasing $\Delta\rho$ is to increase the overall scattering intensity, the increase in $\Delta\rho_u$ ($= \rho_u - \rho_a$), the electron density difference between the amorphous background (ρ_u) and the amorphous lamellae, has the concurrent effects of raising the low-angle intensity (at q values lower than the peak center) and lowering the peak definition. **Fig. 2F** shows the Lorentz-corrected SAXS patterns of the starch samples. The 0.1% and 0.5% alkali solutions for different times resulted in an increase in the low-angle intensity but a decrease in the peak definition. This suggests that alkali increased $\Delta\rho_u$ by inducing a lower destruction to the amorphous background (*i.e.*, amorphous growth rings) than that

295 to the amorphous lamellae. In other words, both lamellar and non-lamellar amorphous starch could
296 be affected by alkali.

297 Also, the scattering at q values lower than the peak position (*ca*. 0.01-0.04 $Å^{-1}$) showed an
298 increase after alkali treatment especially at 0.5% concentration (**Fig. 2F**). This was related to the
299 evolution of a structure with a size of R_{g2}. Here, the alkali certainly disrupted the semicrystalline
300 lamellae, phasing out starch molecules from the lamellae (Zhang, et al., 2015b) to form mass fractals
301 with R_{g2}. This was another reason for the R_{g2} increase after the 0.5% alkali treatment (see **Table 1**).

302 **Table 2** shows the average thicknesses of the semi-crystalline (d), crystalline (d_c) and
303 amorphous (d_a) lamellae. While a slight increase in d was seen after 0.1% alkali treatment, the 0.5%
304 alkali induced a greater increase in d; there was an increase in d_c and a decrease in d_a. Thus, alkali
305 made the semi-crystalline lamellae thicker by swelling the crystalline lamellae rather than the
306 amorphous lamellae. Specifically, alkali ions penetrated into the starch granule to partially break the
307 hydrogen bonding of starch orders such as crystallites, leading to the movement of double helices in
308 crystalline lamellae and thus an increase in d_c. Also, alkali induced out-phasing of starch molecules
309 from the amorphous lamellae and made the amorphous lamellae thinner. This is unlike a previous
310 finding (Thys, et al., 2008) that alkali makes semi-crystalline lamellae thinner for C-polymorphic
311 starch (a hybrid of A- and B-polymorphs). These results demonstrated that alkali increased the semi-
312 crystalline lamellar thickness for the starch with a single A-polymorph.

313 Like for A_{peak} and I_{peak}, the 0.5% alkali treatment with a longer time (12 days) reduced the
314 degrees of the increase in d_c and the decrease in d_a, as compared to the counterpart treatment for 6
315 days. That is, the 0.5% alkali could cause swelling (other than molecular out-phasing) for the
316 amorphous lamellae, contributing to increasing d_a, and also induce molecular realignment
317 (accompanying the lamellae disruption) within the crystalline lamellae, *i.e.*, a decrease in d_c.

318 *3.4 Crystalline structure*

The polarized light micrographs of untreated and alkali-treated starch granules are shown in **Fig. 3A**. Untreated starch granules showed typical polarization crosses, the intensity of which is related to the crystallinity and the microcrystalline orientation of starch (Zhang, et al., 2014c). The cross was almost unchanged after the 0.1% alkali treatment, but the integrity of part of polarization crosses could be broken by the stronger (0.5%) alkali. That is, the stronger alkali partially disorganized the starch crystallites.

Fig. 3B shows the XRD patterns for the starch samples before and after alkali treatment. The untreated starch displayed a typical A-type crystalline structure, as confirmed by intense diffraction peaks at *ca.* 15° and 23° (2θ) and an unresolved doublet at *ca.* 17° and 18°. The alkali treatment induced no change to the polymorphic type, which was in agreement with previous findings (Cai, et al., 2014; Cardoso, Putaux, Samios, & da Silveira, 2007; Jiang, et al., 2014; Wang, et al., 2012). **Table 3** presents the relative crystallinity (X_c). The alkali treatment especially at high concentration (0.5%) decreased X_c. Crystallite disruption is usually seen for alkali-treated starch (Cardoso, et al., 2007; Thys, et al., 2008; Wang, et al., 2012). Again, the time increase under 0.5% alkali condition resulted in a less evident reduction in X_c. Accounting for this, during this stronger alkali treatment, starch multi-scale structure, *e.g.*, lamellae and crystallites, were apparently disrupted, which promoted the leaching (*i.e.*, out-phasing) of amorphous molecular fractions from starch structures, accompany by the formation of starch orders with an increased stability (DSC analysis).

3.5 Thermal behaviors

The DSC thermograms for the starch subjected to the alkali treatment are shown in **Fig. 3C**. An endotherm G was observed for the untreated starch, corresponding to the melting of the short- and long-range molecular orders of the starch, *i.e.*, crystallites and double-helices (Liu, Yu, Xie, & Chen, 2006). The thermal parameters of the starch samples are recorded in **Table 3**. The enthalpy ΔH was positive to the quantity of melted starch molecular orders, which showed a changing trend similar to that of starch crystallinity.

After the 0.1% alkali treatment, the starch showed decreases in the onset (T_o) and peak (T_p) temperatures. Specifically, this mild alkali treatment only reduced the perfection of part of starch orders especially those containing flaws (*i.e.*, reduced T_o and T_p) rather than totally disrupted them (confirmed by slightly reduced X_c and ΔH). Besides, the increase in T_c confirmed the formation of a proportion of starch orders with a higher thermal stability. Then, the transition temperature range ΔT ($=T_c-T_o$) was widened by mild (0.1%) alkali.

With stronger (0.5%) alkali treatment, the starch displayed evident increases in T_o and T_p. This stronger alkali sufficiently disorganized part of starch orders with flaws (shown by prominent reductions in X_c and ΔH). Otherwise, those orders would show low T_o and T_p. Again, starch orders with a greater thermal stability (shown by a moderately increased T_c) emerged. In this way, the apparent increase in T_o and the modest increase in T_c led to a narrowed ΔT. These evolutions were similar to the changes in the molecular orders and thermal parameters of starch induced by heat-moisture treatment (Hoover, 2010; Zhang, et al., 2014d).

Hence, the multi-scale supramolecular structure assembled by starch molecules with heterogeneity could be altered by alkali, as confirmed by the starch structure disruption, *e.g.*, reduction of molecular orders, disruption of semicrystalline lamellae and weakening of molecular organization within growth rings. Accompanying structural disruption, the molecule out-phasing/swelling occurred with the formation of starch orders with an increased stability.

3.6 Discussion on the digestion rate of starch from a view of structural heterogeneity

3.6.1 Digestion of untreated starch

Fig. 4A shows the typical digestion curve and LOS plots, along with their fit curves, for the native (untreated) starch. **Table 4** records the parameters of starch digestion. The LOS model described starch digestion process accurately, as the residuals deduced from the fit data and the digestion data were in the range of −2~2 (%). The LOS plots displayed two linear ranges, identified by different rate constants (*i.e.*, k_1 and k_2). This indicated that native starch showed a dual-phase

digestion, with the first phase having a higher digestion rate than the second one ($k_1 > k_2$). k_2 was just *ca*. 2/5 that of k_1. At the end of the first digestion phase, *ca.* 64.03% (C_{t1}) of the starch could be rapidly hydrolyzed at a rate k_1 (*cf*. **Table 4)**. Since the amorphous fractions of native starch was just *ca.* 50.79% (*cf*. **Table 3**), the digestion at the first phase was proposed to occur in both the amorphous matrix and part of the molecular orders (A-type crystallites, *etc*.).

The dual-phase digestion for native starch could be attributed to the heterogeneity of the multi-scale supramolecular structure assembled by starch molecules. In fact, there were numerous pores on the starch granule surface (*cf*. **Fig. 1**), which connected the granule surface to the interior (hilum) (Chen, et al., 2009). Such pores allowed the penetration of α-amylase molecules with a size of *ca.* 6 nm (Payan, et al., 1980) into the granule interior (Dhital, Butardo, Jobling, & Gidley, 2015). The A-polymorphic starch had numerous short amylopectin side chains (Hizukuri, 1985) and branch points scattered in both the amorphous and crystalline regions. The short double helices (from the short side chains) and the branch linkages in the crystallites led to the formation of flaws, *i.e*., "weak points" (Jane, Wong, & McPherson, 1997), for the starch crystallites. Consequently, the untreated starch contained a large quantity of loosely-packed starch molecules (*i.e*., amorphous matrix and orders with flaws) in the hilum, in the growth rings (including blocklets and mass fractals), in the granule surface, and close to the pores. These fractions were highly susceptible to the enzyme and could be rapidly degraded at the same rate at the first phase. This finding was different from previous investigations which showed amorphous starch is more susceptible to enzyme digestion, whereas ordered starch is less easily hydrolyzed by an enzyme (digestible at a rather lower rate or indigestible) unless they are disrupted (Lopez-Rubio, Htoon, & Gilbert, 2007).

At the end of second phase, approx. 85.78% (C_{t2}) of the starch was hydrolyzed. Here, we propose that part of the densely- packed matrix of the remainder starch, *e.g.*, crystallites containing fewer flaws (than the orders digested at the first phase), could be slowly bound and hydrolyzed by the enzyme at the second phase. This densely-packed matrix had a much lower rate (k_2, *ca.* $0.4 \times k_1$)

than k_1. It is worth mentioning that with starch digestion proceeding, the enzyme concentration reduction and the enzyme deactivation were unavoidable. As this work was mainly focused on how the starch multi-scale structure (also with alkali treatment) with heterogeneity affects the starch digestion rate, those enzyme-related factors would not be discussed in the following.

3.6.2 Digestion of alkali-treated starch

The digestion curves, LOS plots and fit curves for the alkali-treated starch samples are presented in **Fig. 4B-E**. The digestion parameters are summarized in **Table 4**. With the 0.1% alkali treatment, the LOS plots retained the two linear ranges. Compared to the untreated starch, the alkali-treated starch could be digested to a similar extent (C_{t1}) ($P > 0.05$) at a similar rate (k_1) at the first stage, and to an increased digestion extent (C_{t2}) at a slightly changed k_2 at the second phase. The increased treatment time did not induce additional changes to the digestion rates (k_1 and k_2) and extents (C_{t1} and C_{t2}). When a higher (0.5%) alkali concentration was used, a digestion course with three different rates (*i.e.*, a triple-phase digestion pattern) ($k_1 > k_2 > k_3$; **Fig. 4D** and **E**, and **Table 4**) was observed for the alkali-treated starch samples. The samples with 0.5% alkali treatment had much higher k_1 and k_2 than did those with 0.1% alkali treatment, indicating enhanced starch digestibility. In additon, with a longer treatment time (12 days), the 0.5% alkali caused less increases in digestion rates (k_1 and k_2) but relatively stable digestion proportions (C_{t1} and C_{t2}) at the first and second digestion phases. At the third digestion phase, the digestion rate (k_3) and proportion (C_{t3}) were almost unchanged.

As the same starch and amylase were used, the alkali-induced evolutions in the digestion kinetics of starch should result from the changes in the heterogeneity of starch multi-scale supramolecular structure. The alkali treatment of the starch acted in several steps, including the alkali penetration into the granule interior, the alkali-induced disruption (with swelling and molecular reassembly) in the multi-scale structure, and the out-phasing (leaching, *etc*.) of starch molecules from the structure.

The 0.1% alkali solution moderately altered the heterogeneous starch structures on multiple scales. (a) Part of starch molecular orders, *i.e*., crystallites and helices, were slightly disrupted

(reduced X_c and ΔH) with reduced perfection (decreased T_o); and certain molecular chains reassembled to form new orders with increased thermal stability (increased T_c). (b) The crystalline lamellae were swollen (increased d_c) by weakening alignment of double helices within the lamellae, while the out-phasing of starch molecules occurred for amorphous lamellae and reduced their thickness d_a. (c) Then, there was a decrease in the compactness of molecular organization within the growth rings, as disclosed by reduced δ_1. Also, this alkali caused molecular leaching/out-phasing from superficial and internal regions of the granules, the blocklets and the mass fractals, leading to reduced granule size and R_{g2}. Also, the granule pores were enlarged. Consequently, these modest changes in the starch hierarchical structure could transform part of perfect starch orders that are intrinsic resistant to the enzyme into mainly molecular orders with a small amount of flaws. Those orders, contained a small amount of flaws, could be bound and digested by the amylase at a slow rate k_2. Thus, at the end of the second digestion phase, the proportion (C_{t2}) of digestible amorphous and ordered components was increased from *ca.* 85% to > 90% (*cf.* **Table 4**), though the digestion rates at dual phases almost remained unchanged. Besides, the increased time did not cause additional alterations to the multi-scale supramolecular structure, and thus led to no difference in the digestion rates for the 0.1% alkali treated samples.

However, with stronger (0.5%) alkali treatment, the starch supramolecular structure with heterogeneity underwent more prominent evolutions. In particular, part of starch orders could be sufficiently disorganized (apparently reduced X_c and ΔH). The swelling of crystalline lamellae and the molecular out-phasing from crystalline lamellae were enhanced, accompanied by evidently reduced lamellae ordering. Moreover, the whole granule, the blocklets and the mass fractals could be apparently swelling, as seen by increased granule size and R_{g2}. These drastically-weakened molecular packing of starch on multiple scales resulted in the emergence of a starch fraction with an intermediate digestion rate k_2 ($k_1 > k_2 > k_3$, *cf.* **Fig. 4D-E** and **Table 4**). That is: 1) part of perfect starch orders that are resistant to amylase became mainly orders with a small amount of flaws, which

showed a slow digestion rate k_3 similar to k_2 of the untreated starch; 2) part of original orders with a small amount of flaws showed a further reduced perfection and probably formed amorphous material, with an intermediate digestion rate k_2 which was slightly higher than k_1 of the untreated starch; 3) predominantly amorphous starch packed in the multi-scale structure were swollen apparently and thus had a drastically-accelerated digestion rate k_1 that was evidently higher than k_1 of the untreated starch. Interestingly, an increase in treatment time with this stronger (0.5%) alkali enhanced packing of starch molecules in the multi-scale structure by inducing the formation of starch orders with an increased thermal stability. These orders reduced the accessibility of starch molecules to the enzyme, resulting in evidently reduced digestion rates (k_1 and k_2) at the first and second phases and negligibly altered the digestion rate (k_3) at the third phase and the digestion proportions at all the phases (C_{t1}, C_{t2}, and C_{t3}).

4. Conclusions

The link between the multi-scale supramolecular structure of starch and its multi-phase digestion rates was established from a view of structure heterogeneity. Specifically, the untreated starch showed a dual-phase digestion, suggesting two digestible fractions (within the heterogeneous supramolecular structure) with different hydrolysis rates. At the first phase, both amorphous starch and part of molecular orders (crystallites with flaws, *etc*.) were digested at the same rate; at the second phase, the densely-packed starch, *e.g.*, orders containing fewer flaws, was digested rather slowly. Furthermore, alkali altered starch digestion behaviors by changing the heterogeneity of the starch supramolecular structure on multiple scales. Mild alkali treatment slightly disrupted the starch multi-scale structure, which transformed a small part of resistant starch into slowly-digestible fraction rather than increased the digestion rates. Stronger alkali treatment (increased alkali concentration) led to the emergence of a triple-phase digestion with increased digestion rates for starch, by apparently weakening the multi-scale structure. Moreover, the formation of starch orders with an enhanced thermal stability, especially induced by the stronger alkali, reduced starch digestion

rate with the treatment time. This work enables a further understanding of the digestion rate of starch, which is of value for the design and development of starchy foods with tailored digestibility.

Acknowledgments

The authors would like to acknowledge the Fundamental Research Funds for the Central Universities (2662016QD008), the Open Project Program of Provincial Key Laboratory of Green Processing Technology and Product Safety of Natural Products (Nos. 201602 and 201604), the National Natural Science Foundation of China (No. 31401586), and the Hunan Province Science and Technology Key Project (No. 2014FJ1008). This research was partly undertaken on the SAXS/WAXS beamline at the Australian Synchrotron, Victoria, Australia.

References

Bertoft, E., & Manelius, R. (1992). A method for the study of the enzymic hydrolysis of starch granules. *Carbohydrate Research, 227*, 269-283.

Blazek, J., & Gilbert, E. P. (2010). Effect of Enzymatic Hydrolysis on Native Starch Granule Structure. *Biomacromolecules, 11*(12), 3275-3289.

Cai, J., Yang, Y., Man, J., Huang, J., Wang, Z., Zhang, C., Gu, M., Liu, Q., & Wei, C. (2014). Structural and functional properties of alkali-treated high-amylose rice starch. *Food Chemistry, 145*, 245-253.

Cameron, R. E., & Donald, A. M. (1993). A Small-Angle X-Ray-Scattering Study of Starch Gelatinization in Excess and Limiting Water. *Journal of Polymer Science Part B-Polymer Physics, 31*(9), 1197-1203.

Cardoso, M. B., Putaux, J.-L., Samios, D., & da Silveira, N. P. (2007). Influence of alkali concentration on the deproteinization and/or gelatinization of rice starch. *Carbohydrate Polymers, 70*(2), 160-165.

Chen, P., Wang, K., Kuang, Q., Zhou, S., Wang, D., & Liu, X. (2016). Understanding how the aggregation structure of starch affects its gastrointestinal digestion rate and extent. *International Journal of Biological Macromolecules, 87*, 28-33.

Chen, P., Yu, L., Simon, G., Petinakis, E., Dean, K., & Chen, L. (2009). Morphologies and microstructures of cornstarches with different amylose-amylopectin ratios studied by confocal laser scanning microscope. *Journal of Cereal Science, 50*(2), 241-247.

Chung, H. J., Lim, H. S., & Lim, S. T. (2006). Effect of partial gelatinization and retrogradation on the enzymatic digestion of waxy rice starch. *Journal of Cereal Science, 43*(3), 353-359.

Dhital, S., Butardo, V. M., Jobling, S. A., & Gidley, M. J. (2015). Rice starch granule amylolysis–Differentiating effects of particle size, morphology, thermal properties and crystalline polymorph. *Carbohydrate Polymers, 115*, 305-316.

Doutch, J., & Gilbert, E. P. (2013). Characterisation of large scale structures in starch granules via small-angle neutron and X-ray scattering. *Carbohydrate Polymers, 91*(1), 444-451.

Han, J.-A., & Lim, S.-T. (2004). Structural changes in corn starches during alkaline dissolution by vortexing. *Carbohydrate Polymers, 55*(2), 193-199.

Hasjim, J., Lavau, G. C., Gidley, M. J., & Gilbert, R. G. (2010). In vivo and in vitro starch digestion: Are current in vitro techniques adequate? *Biomacromolecules, 11*(12), 3600-3608.

Hizukuri, S. (1985). Relationship between the distribution of the chain length of amylopectin and the crystalline structure of starch granules. *Carbohydrate Research, 141*(2), 295-306.

Hoover, R. (2010). The impact of heat-moisture treatment on molecular structures and properties of starches isolated from different botanical sources. *Critical Reviews in Food Science and Nutrition, 50*(9), 835-847.

Jane, J.-l., Wong, K.-s., & McPherson, A. E. (1997). Branch-structure difference in starches of A-and B-type X-ray patterns revealed by their Naegeli dextrins. *Carbohydrate Research, 300*(3), 219-227.

Jiang, Q., Gao, W., Li, X., Man, S., Shi, Y., Yang, Y., Huang, L., & Liu, C. (2014). Comparative susceptibilities to alkali-treatment of A-, B-and C-type starches of Dioscorea zingiberensis, Dioscorea persimilis and Dioscorea opposita. *Food Hydrocolloids, 39*, 286-294.

Juansang, J., Puttanlek, C., Rungsardthong, V., Puncha-arnon, S., & Uttapap, D. (2012). Effect of gelatinisation on slowly digestible starch and resistant starch of heat-moisture treated and chemically modified canna starches. *Food Chemistry, 131*(2), 500-507.

Kuang, Q., Xu, J., Liang, Y., Xie, F., Tian, F., Zhou, S., & Liu, X. (2017). Lamellar structure change of waxy corn starch during gelatinization by time-resolved synchrotron SAXS. *Food Hydrocolloids, 62*, 43-48.

Liu, H., Yu, L., Xie, F., & Chen, L. (2006). Gelatinization of cornstarch with different amylose/amylopectin content. *Carbohydrate Polymers, 65*(3), 357-363.

Liu, W. C., Halley, P. J., & Gilbert, R. G. (2010). Mechanism of Degradation of Starch, a Highly Branched Polymer, during Extrusion. *Macromolecules, 43*(6), 2855-2864.

Lopez-Rubio, A., Htoon, A., & Gilbert, E. P. (2007). Influence of extrusion and digestion on the nanostructure of high-amylose maize starch. *Biomacromolecules, 8*(5), 1564-1572.

McDougall, G. J., Shpiro, F., Dobson, P., Smith, P., Blake, A., & Stewart, D. (2005). Different polyphenolic components of soft fruits inhibit α-amylase and α-glucosidase. *Journal of Agricultural and Food Chemistry, 53*(7), 2760-2766.

Nadiha, M. N., Fazilah, A., Bhat, R., & Karim, A. A. (2010). Comparative susceptibilities of sago, potato and corn starches to alkali treatment. *Food Chemistry, 121*(4), 1053-1059.

Noda, T., Takigawa, S., Matsuura-Endo, C., Suzuki, T., Hashimoto, N., Kottearachchi, N. S., Yamauchi, H., & Zaidul, I. S. M. (2008). Factors affecting the digestibility of raw and gelatinized potato starches. *Food Chemistry, 110*(2), 465-470.

Nwosu, F., Morris, J., Lund, V. A., Stewart, D., Ross, H. A., & McDougall, G. J. (2011). Anti-proliferative and potential anti-diabetic effects of phenolic-rich extracts from edible marine algae. *Food Chemistry, 126*(3), 1006-1012.

Payan, F., Haser, R., Pierrot, M., Frey, M., Astier, J., Abadie, B., Duée, B., & Buisson, G. (1980). The three-dimensional structure of α-amylase from porcine pancreas at 5 Å resolution–The active-site location. *Acta Crystallographica Section B Structural Crystallography and Crystal Chemistry, 36*(2), 416-421.

Perez, S., & Bertoft, E. (2010). The molecular structures of starch components and their contribution to the architecture of starch granules: A comprehensive review. *Starch-Starke, 62*(8), 389-420.

Poulsen, B. R., Ruiter, G., Visser, J., & Iversen, J. J. L. (2003). Determination of first order rate constants by natural logarithm of the slope plot exemplified by analysis of Aspergillus niger in batch culture. *Biotechnology Letters, 25*(7), 565-571.

Praznik, W., Buksa, K., Ziobro, R., Gambuś, H., & Nowotna, A. (2012). The effect of long‐term alkali treatment on the molecular characteristics of native and extruded starches at 35° C. *Starch‐Stärke*, *64*(11), 890-897.

Robertson, M., Currie, J., Morgan, L., Jewell, D., & Frayn, K. (2003). Prior short-term consumption of resistant starch enhances postprandial insulin sensitivity in healthy subjects. *Diabetologia*, *46*(5), 659-665.

Tamura, M., Singh, J., Kaur, L., & Ogawa, Y. (2016). Impact of structural characteristics on starch digestibility of cooked rice. *Food Chemistry*, *191*, 91-97.

Tan, I., Flanagan, B. M., Halley, P. J., Whittaker, A. K., & Gidley, M. J. (2007). A method for estimating the nature and relative proportions of amorphous, single, and double-helical components in starch granules by C-13 CP/MAS NMR. *Biomacromolecules*, *8*(3), 885-891.

Thys, R. C., Westfahl Jr, H., Noreña, C. P., Marczak, L. D., Silveira, N. P., & Cardoso, M. B. (2008). Effect of the alkaline treatment on the ultrastructure of C-type starch granules. *Biomacromolecules*, *9*(7), 1894-1901.

Wang, S., & Copeland, L. (2012). Effect of alkali treatment on structure and function of pea starch granules. *Food Chemistry*, *135*(3), 1635-1642.

Wang, S. J., Sun, Y., Wang, J. R., Wang, S., & Copeland, L. (2016). Molecular disassembly of rice and lotus starches during thermal processing and its effect on starch digestibility. *Food & function*, *7*(2), 1188-1195.

Witt, T., Doutch, J., Gilbert, E. P., & Gilbert, R. G. (2012). Relations between molecular, crystalline, and lamellar structures of amylopectin. *Biomacromolecules*, *13*(12), 4273-4282.

Yang, Z., Swedlund, P., Hemar, Y., Mo, G., Wei, Y., Li, Z., & Wu, Z. (2016). Effect of high hydrostatic pressure on the supramolecular structure of corn starch with different amylose contents. *International Journal of Biological Macromolecules*, *85*, 604-614.

Zhang, B., Chen, L., Li, X., Li, L., & Zhang, H. (2015a). Understanding the multi-scale structure and functional properties of starch modulated by glow-plasma: A structure-functionality relationship. *Food Hydrocolloids*, *50*, 228-236.

Zhang, B., Dhital, S., & Gidley, M. J. (2013). Synergistic and antagonistic effects of α-amylase and amyloglucosidase on starch digestion. *Biomacromolecules*, *14*(6), 1945-1954.

572 Zhang, B., Wang, K., Hasjim, J., Li, E., Flanagan, B. M., Gidley, M. J., & Dhital, S. (2014a). Freeze-drying
573 changes the structure and digestibility of B-polymorphic starches. *Journal of Agricultural and Food*
574 *Chemistry, 62*(7), 1482-1491.
575 Zhang, B. J., Chen, L., Xie, F. W., Li, X. X., Truss, R. W., Halley, P. J., Shamshina, J. L., Rogers, R. D., &
576 McNally, T. (2015b). Understanding the structural disorganization of starch in water-ionic liquid solutions.
577 *Physical Chemistry Chemical Physics, 17*, 13860-13871.
578 Zhang, B. J., Chen, L., Zhao, Y., & Li, X. X. (2013). Structure and enzymatic resistivity of debranched high
579 temperature-pressure treated high-amylose corn starch. *Journal of Cereal Science, 57*(3), 348-355.
580 Zhang, B. J., Xiong, S. X., Li, X. X., Li, L., Xie, F. W., & Chen, L. (2014b). Effect of oxygen glow plasma on
581 supramolecular and molecular structures of starch and related mechanism. *Food Hydrocolloids, 37*, 69-76.
582 Zhang, B. J., Zhao, Y., Li, X. X., Li, L., Xie, F. W., & Chen, L. (2014c). Supramolecular structural changes of
583 waxy and high-amylose cornstarches heated in abundant water. *Food Hydrocolloids, 35*, 700-709.
584 Zhang, B. J., Zhao, Y., Li, X. X., Zhang, P. F., Li, L., Xie, F. W., & Chen, L. (2014d). Effects of amylose and
585 phosphate monoester on aggregation structures of heat-moisture treated potato starches. *Carbohydrate*
586 *Polymers, 103*, 228-233.
587 Zou, W., Sissons, M., Gidley, M. J., Gilbert, R. G., & Warren, F. J. (2015). Combined techniques for
588 characterising pasta structure reveals how the gluten network slows enzymic digestion rate. *Food*
589 *Chemistry, 188*, 559-568.
590
591
592
593

611 **Table 1** Granule size distribution and large-scale parameters of native and alkali-treated starch (S) samples

612 (first-level covers *q*-range *ca.* 0.0020 to 0.01 Å^{-1}; second-level *q*-range *ca.* 0.01 to 0.04 Å^{-1}) [A]

	S	S-0.1-6	S-0.1-12	S-0.5-6	S-0.5-12
P_{D1} (%)	6.75±0.11 [c]	10.80±0.17 [b]	13.75±0.13 [a]	6.92±0.35 [c]	6.52±0.19 [d]
P_{D2} (%)	86.97±0.24 [b]	89.20±0.17 [a]	86.24±0.13 [c]	35.28±0.45 [e]	47.70±0.27 [d]
P_{D3} (%)	6.28±0.13 [c]	0.00±0.00 [d]	0.00±0.00 [d]	57.80±0.80 [a]	45.78±0.46 [b]
δ_1	3.31±0.00 [a]	3.12±0.00 [c]	3.16±0.00 [b]	3.00±0.00 [e]	3.09±0.00 [d]
R_{g1} (Å)	1065.32±8.82 [b]	1062.17±8.06 [c]	1076.92±8.61 [a]	1022.78±8.96 [e]	1046.56±9.89 [d]
δ_2	0.95±0.00 [d]	0.96±0.00 [c]	0.92±0.00 [e]	1.58±0.00 [b]	1.60±0.00 [a]
R_{g2} (Å)	195.36±1.85 [c]	185.67±1.97 [d]	187.38±1.95 [d]	237.40±2.41 [a]	232.30±2.42 [b]

613 [A] Parameters obtained by laser diffraction: P_{D1}, P_{D2}, and P_{D3} are the proportions of starch granules in the

614 diameter ranges of < 7, 7-28, and > 28 µm, respectively. Large-scale structural parameters fitted from SAXS

615 data: δ_1 and δ_2, power law exponents for the first- and second-level *q*-ranges, respectively; R_{g1} and R_{g2},

616 radiuses of gyration for the first- and second-level *q*-ranges, respectively. Values are means of three

617 determinations (n = 3) values. The different inline letter within a row means significant difference (P < 0.05).

618 **Table 2** Lamellar parameters of native and alkali-treated starch (S) samples [A]

	S	S-0.1-6	S-0.1-12	S-0.5-6	S-0.5-12
A_{peak} (a.u.)	3.62±0.15 [c]	4.38±0.12 [b]	4.50±0.12 [a]	1.76±0.05 [e]	2.04±0.07 [d]
I_{peak} (a.u.)	85.68±0.31 [c]	103.60±0.38 [b]	106.33±0.37 [a]	44.03±0.22 [e]	50.20±0.23 [d]
Chi^2	4.06	2.27	2.37	0.69	1.03
d (nm)	9.15±0.00 [d]	9.20±0.00 [c]	9.20±0.00 [c]	9.25±0.00 [a]	9.23±0.00 [b]
d_a (nm)	2.83±0.01 [a]	2.78±0.00 [b]	2.79±0.01 [b]	2.68±0.01 [d]	2.74±0.01 [c]
d_c (nm)	6.32±0.01 [d]	6.42±0.00 [c]	6.41±0.01 [c]	6.57±0.01 [a]	6.49±0.01 [b]

619 [A] Lamellar parameters fitted from SAXS data: A_{peak}, area of lamellar peak, respectively; I_{peak}, area of lamellar
620 peak; Chi^2, reduced chi square. Lamellar parameters obtained by SAXS coupled with 1D correlation function:
621 d, average thickness of semicrystalline lamellae; d_a, average thickness of amorphous lamellae; d_c, average
622 thickness of crystalline lamellae. Values are means of three determinations (n = 3) values. The different inline
623 letter within a row means significant difference ($P < 0.05$).

624 **Table 3** Crystalline and thermal parameters of native and alkali-treated starch (S) samples [A]

	S	S-0.1-6	S-0.1-12	S-0.5-6	S-0.5-12
X_c (%)	49.21±0.68 [a]	47.31±0.75 [b]	44.70±1.02 [c]	39.62±1.10 [e]	42.52±0.96 [d]
T_o (°C)	72.31±0.20 [b]	68.96±0.35 [c]	67.95±0.19 [d]	77.35±0.23 [a]	77.17±0.37 [a]
T_p (°C)	78.57±0.15 [c]	75.98±0.22 [d]	75.38±0.16 [e]	81.95±0.26 [a]	81.27±0.18 [b]
T_c (°C)	86.14±0.32 [d]	89.11±0.24 [c]	89.88±0.38 [b]	90.06±0.43 [a]	89.73±0.23 [ab]
ΔT (°C)	13.83±0.12 [c]	20.15±0.11 [b]	21.93±0.19 [a]	12.71±0.20 [d]	12.56±0.14 [e]
ΔH (J/g)	15.42±0.16 [a]	15.12±0.21 [b]	14.28±0.38 [c]	10.55±0.26 [e]	11.52±0.22 [d]

625 [A] Parameter obtained by XRD: X_c, relative crystallinity. Thermal transition parameters measured by DSC: T_o,
626 onsite temperature; T_p, peak temperature; T_c, conclusion temperature; ΔT ($T_c - T_o$), transition temperature
627 range; ΔH, transition enthalpy. Values are means of three determinations (n = 3) values. The different inline
628 letter within a row means significant difference ($P < 0.05$).

629 **Table 4** Digestion parameters of native and alkali-treated starch (S) samples [A]

		S	S-0.1-6	S-0.1-12	S-0.5-6	S-0.5-12
Phase I	k_1 (min^{-1})	$(1.03\pm0.01)\times10^{-2\,c}$	$(0.97\pm0.09)\times10^{-2\,c}$	$(0.95\pm0.04)\times10^{-2\,c}$	$(4.36\pm0.35)\times10^{-2\,a}$	$(2.76\pm0.09)\times10^{-2\,b}$
	t_1 *(min)*	180±0 ^{a}	180±0 ^{a}	180±0 ^{a}	40±0 ^{c}	50±0 ^{b}
	C_{t1} (%)	64.03±1.49 ^{a}	63.93±0.51 ^{a}	65.74±2.05 ^{a}	49.23±0.44 ^{b}	50.59±1.08 ^{b}
Phase II	k_2 (min^{-1})	$(0.44\pm0.01)\times10^{-2\,c}$	$(0.41\pm0.01)\times10^{-2\,d}$	$(0.41\pm0.02)\times10^{-2\,cd}$	$(1.48\pm0.21)\times10^{-2\,a}$	$(0.94\pm0.13)\times10^{-2\,b}$
	t_2 *(min)*	540±0 ^{a}	540±0 ^{a}	540±0 ^{a}	180±0 ^{a}	180±0 ^{a}
	C_{t2} (%)	85.78±1.45 ^{b}	92.08±0.65 ^{a}	95.50±2.49 ^{a}	75.92±0.49 ^{c}	76.88±2.00 ^{c}
Phase III	k_3 (min^{-1})	--	--	--	$(0.56\pm0.05)\times10^{-2\,a}$	$(0.48\pm0.08)\times10^{-2\,a}$
	t_3 *(min)*	--	--	--	540±0 ^{a}	540±0 ^{a}
	C_{t3} (%)	--	--	--	96.56±1.04 ^{a}	95.47±2.18 ^{a}

630 [A] k_1, k_2 *and* k_3 are the rate constants for the first, second and third phases of digestion; t_1, t_2 and t_3 are the times
631 required for the first, second and third phases of digestion; C_{t1},C_{t2} and C_{t3} are the digested proportions of
632 starch at the first, second and third phases of digestion. Values are means of three determinations (n = 3)
633 values. The different inline letter within a row means significant difference ($P < 0.05$).

Figure Captions

Fig. 1 SEM images of native and alkali-treated starch (S) granules.

Fig. 2 Double-logarithmic SAXS patterns and their fit curves (A-E), and Lorentz corrected SAXS patterns (F) of native and alkali-treated starch (S) samples.

Fig. 3 Polarized-light micrographs (A), XRD patterns (B) and DSC thermograms (C) of native and alkali-treated starch (S) samples.

Fig. 4 Typical digestion curves, LOS plots and fit curves for native and alkali-treated starch (S) samples. ○, Experiment data; ×, □ and ☆, LOS plot data in first, second and third phases respectively; ——, linear fit curve for LOS plot data; —— , —— and – – , fit curve based on the slope and intercept values of the linear fit curve for LOS plot in first, second and third phases, respectively.

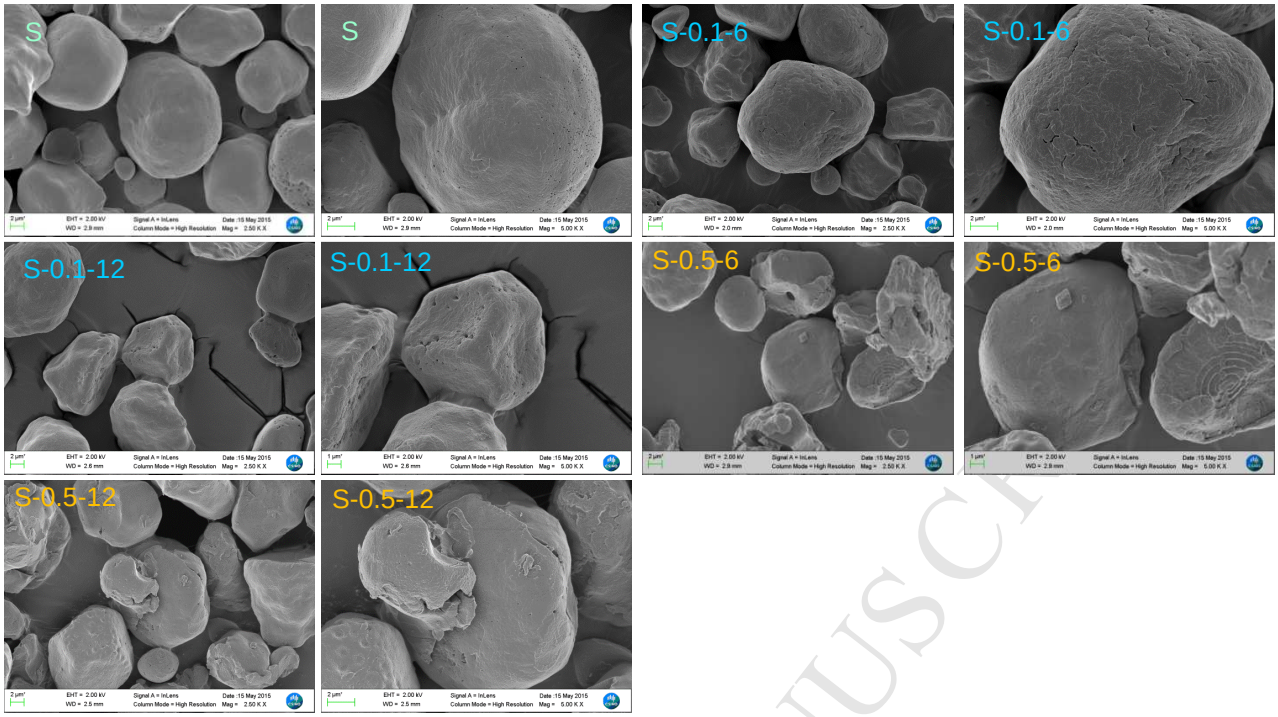

604 **Fig. 1**

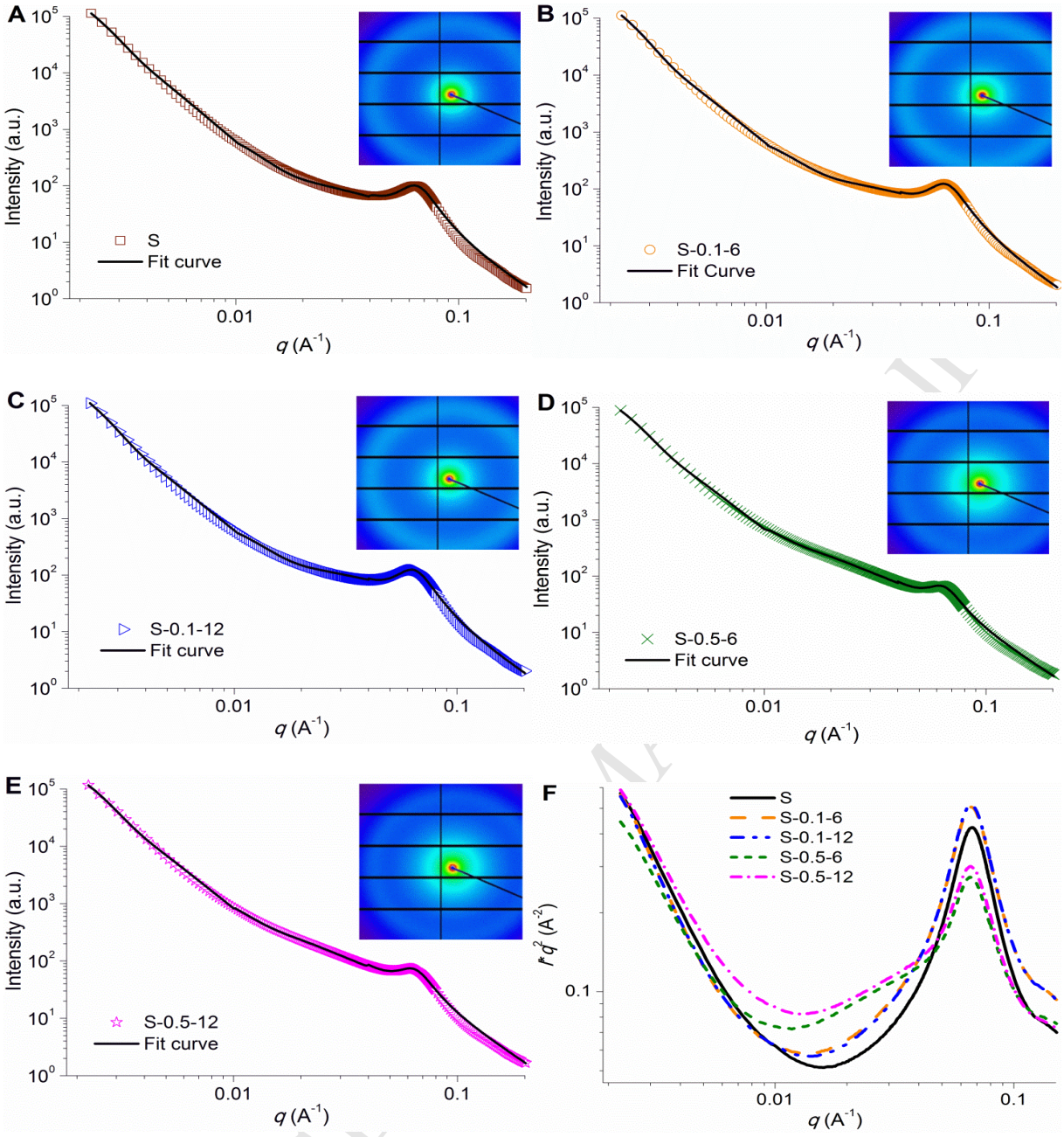
A
Intensity (a.u.)
S
Fit curve
q (A-1)
B
S-0.1-6
Fit Curve
C
S-0.1-12
Fit curve
D
S-0.5-6
Fit curve
E
S-0.5-12
Fit curve
F
S
S-0.1-6
S-0.1-12
S-0.5-6
S-0.5-12
I*q2 (A-2)

Fig. 2

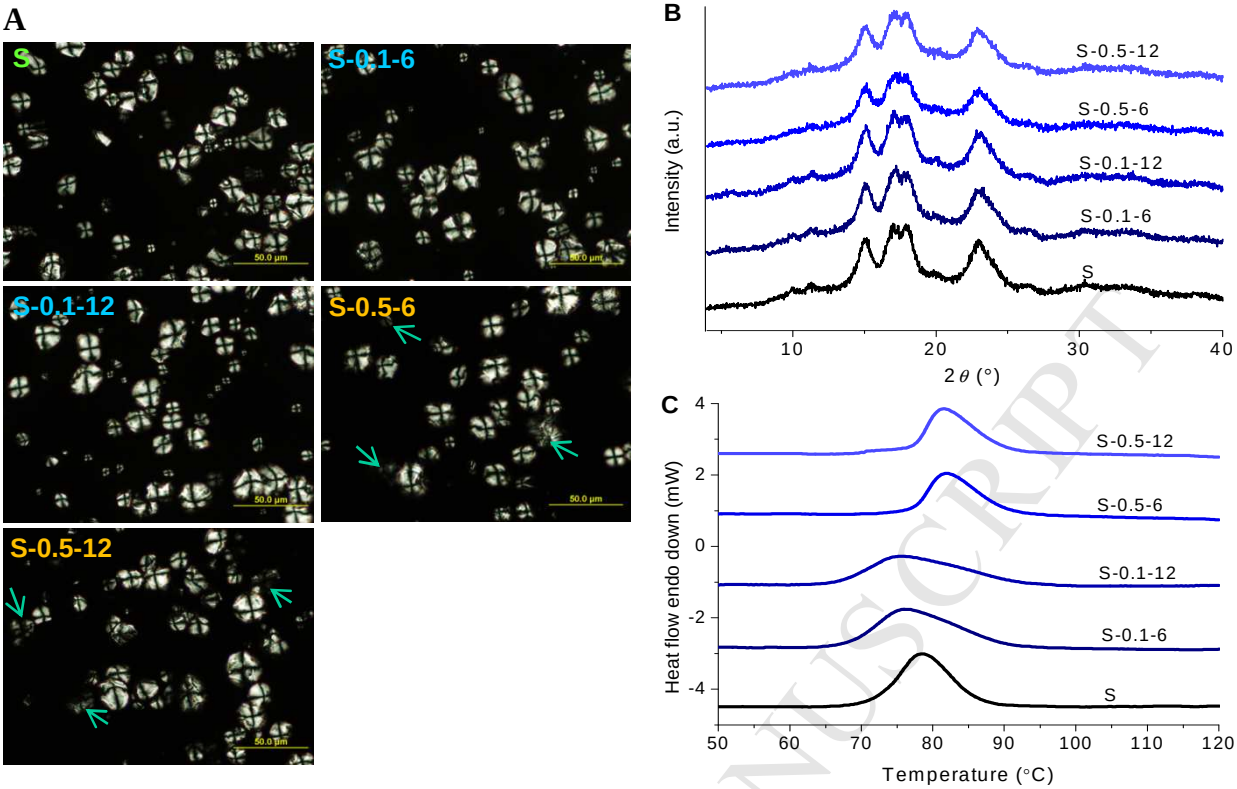

609 **Fig. 3**

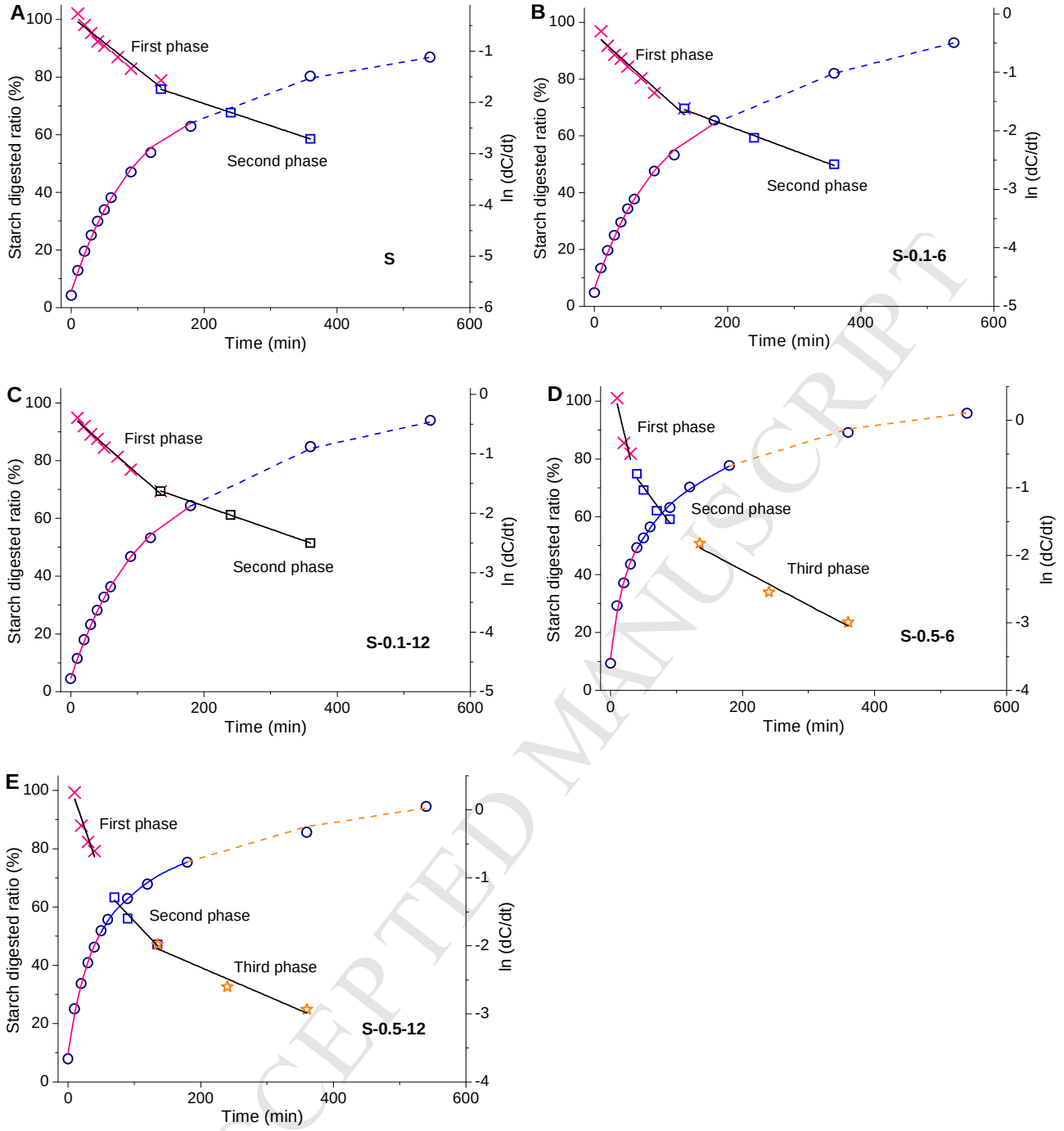

610 **Fig. 4**

Highlights

- Relation between supramolecular structure and digestion rate was further disclosed.
- Untreated starch had two digestible fractions with different digestion rates.
- Amorphous starch and partial orders could be digested at a same rate.
- Multi-scale structural changes induced by alkali altered starch digestion date.